Remote Sensing of Environment 192 (2017) 217–227

Contents lists available at ScienceDirect

Remote Sensing of Environment

journal homepage: www.elsevier.com/locate/rse

Remote estimation of biomass of *Ulva prolifera* macroalgae in the Yellow Sea

Lianbo Hu [a,*], Chuanmin Hu [b], Ming-Xia HE [a]

[a] Ocean Remote Sensing Institute, Ocean University of China, 5 Yushan Road, Qingdao 266003, China
[b] College of Marine Science, University of South Florida, 140 Seventh Avenue, South, St. Petersburg, FL 33701, United States

ARTICLE INFO

Article history:
Received 18 July 2016
Received in revised form 9 January 2017
Accepted 27 January 2017
Available online 28 February 2017

Keywords:
Ulva prolifera
Green tide
MODIS
Remote sensing
Biomass
Carbon
Nitrogen

ABSTRACT

Since 2008, macroalgal blooms of *Ulva prolifera* (also called green tides) occurred every summer in the Yellow Sea (YS), causing environmental and economic problems. A number of studies have used satellite observations to estimate the severity of the blooms through estimating the bloom size and duration. However, a critical bloom parameter, namely biomass, has never been objectively determined due to lack of measurements. In this study, laboratory experiments were conducted to measure *U. prolifera* biomass (wet weight) per unit area and the corresponding spectral reflectance, through which a robust relationship has been established to link biomass per area to the reflectance-based floating algae index (FAI). The lab-based model has been validated with *in situ* measurements, with an estimated relative uncertainty of <16% for algae with FAI values <0.2 (corresponding to ~2 kg/m^2 biomass and accounting for >99.5% of the algae-containing pixels in satellite images). The model was further transferred to MODIS Rayleigh-corrected reflectance (R_{rc}), where aerosol impacts on the model were simulated under various atmospheric conditions. The simulations showed an average of 6.5% (up to 12.3% for the extreme case) uncertainties in biomass estimates when MODIS R_{rc} data were used as the model inputs. The dry biomass per wet biomass and carbon and nitrogen contents per dry biomass were also determined through lab experiments, thus making their estimation possible from MODIS R_{rc} data. The model was then applied to time-series of MODIS observations over the YS between 2008 and 2015 to determine the inter-annual variability of these critical parameters. Results showed maximum daily biomass of >1.7 million tons during June 2015 and minimum daily biomass of <0.09 million tons during 2012. The ability to estimate *U. prolifera* biomass at given locations from the near real-time MODIS images is expected to significantly enhance the capacity of an existing monitoring system to provide quantitative information for decision making.

1. Introduction

Green tides refer to the abnormal proliferation of floating green macroalgae, which usually occur in the eutrophic waters of bays, lakes, and other coastal waters (Nelson et al., 2003; Charlier et al., 2006; Yabe et al., 2009). In summer 2008, an extensive green tide of *Ulva prolifera* occurred in the Yellow Sea (YS, Fig. 1), especially in coastal waters off Qingdao (China), causing trouble in sailing practice by athletes to prepare for the upcoming Olympic sailing competition. The event caused serious economic losses and environmental problems, and caught national and international attention of news media and scientists (Qingdao News, 2008; Mail Daily, 2008; Hu and He, 2008; Lü and Qiao, 2008; Liang et al., 2008; Liu et al., 2009). Since 2008, similar green tides occurred in the YS every summer. The economic cost for mitigation (beach clean up and algae transportation) and aquaculture losses exceeded 200 million U.S. dollars in 2008 (Wang et al., 2009b; Ye et al., 2011) and 350 million U.S. dollars between 2008 and 2015 (China Marine Disaster Bulletin, 2008–2013). Meanwhile, recurrent green tides caused a series of adverse impacts on the marine environment (Liu et al., 2010; Liu et al., 2013a; Wang et al., 2015), and have been regarded by the Chinese government as another ecological disaster in addition to red tides along China's coasts.

Similar to most other single-species green tides worldwide (Taylor et al., 2001; Nelson et al., 2003), the dominant species of green tides in the YS is *U. prolifera* (Leliaert et al., 2009; Liu et al., 2009; Shen et al., 2012). *U. prolifera* is a seaweed worldwide that can grow rapidly under favorable conditions, leading to extensive blooms (green tides). For the green tides in the YS, satellite remote sensing, ocean circulation models, and field observations all indicate their origin in the Subei Shoal of Jiangsu province (Fig. 1). From the Subei Shoal, although coastal aquaculture ponds have been suggested to be the source of *U. prolifera* (Pang et al., 2010; Liu et al., 2013b), more evidences led to the conclusion that *Porphyra* aquaculture rafts should be the main source of *U. prolifera* (Liu et al., 2009; Hu et al., 2010; Liu et al., 2010; Liu et al., 2013a; Zhang et al., 2014; Wang et al., 2015). The initial *U. prolifera* in

* Corresponding author.
E-mail address: hulb@ouc.edu.cn (L. Hu).

http://dx.doi.org/10.1016/j.rse.2017.01.037

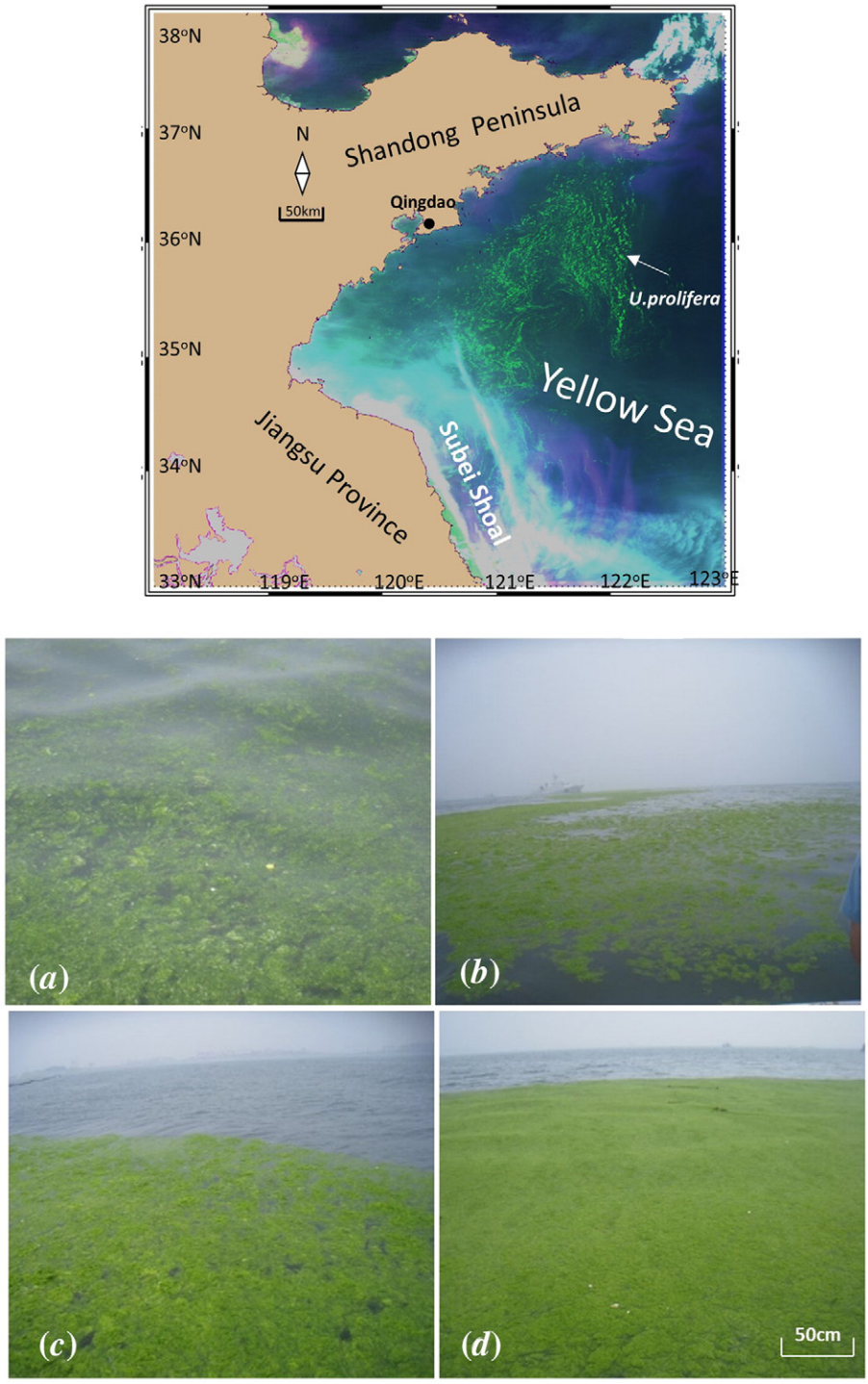

Fig. 1. Top: study region showing the Yellow Sea. The background image is MODIS false color Red-Green-Blue (R:Rrc_645, G: Rrc_859, B:Rrc_469) image on 12 June 2015, which shows the *U. prolifera* algae slicks in greenish colors. Bottom (a–d): digital photos of *U. prolifera* macroalgae floating on the ocean surface taken from boat in coastal waters off Qingdao (black dot in map) during the *in situ* experiment in July 2013.

the Subei Shoal first drifts to the YS following the dominant northward currents, develops into a green tide under favorable sun light and water clarity conditions, and then moves toward the Shandong Peninsula following the southeast monsoon and summer ocean surface currents (Hu et al., 2010; Liu et al., 2010; Keesing et al., 2011; Qiao et al., 2011; Xu et al., 2016).

Among the various methods, satellite remote sensing has been widely used to detect and track green tides in the YS due to it synoptic and frequent coverage. Indeed, the first report of the green tide origin was from analysis of MODIS data, where MODIS normalized difference vegetation index (NDVI) was used to examine image series to track the green tide origin (Hu and He, 2008; Liu et al., 2009). This is because *U. prolifera* is simply a vegetation floating on the sea surface. *U. prolifera* features a hollow tubular body composed of monolayer cells, which release oxygen in the body during photosynthesis. The oxygen increases the algae's buoyancy, making them float on the sea surface (Liang et al., 2008) and form algae mats under the influence of wind and current (Gower et al., 2006; Hu, 2009). Fig. 1a–d show photos of *U. prolifera* with different density floating on the sea surface.

However, because of NDVI's strong sensitivity to atmospheric conditions and observing geometry, it is difficult to use NDVI to quantify green tide coverage (*i.e.*, bloom size). Hu (2009) therefore developed a new index to detect and quantify green tides, namely the floating algae index (FAI), defined as the magnitude of the near-infrared (NIR) reflectance against a linear baseline between the red and shortwave infrared bands. Compared with NDVI, FAI is less sensitive to changes in atmospheric conditions (aerosol optical thickness and type) or in solar/viewing geometry, and it is also less sensitive to perturbations by thin clouds or moderate sun glint. Most importantly, its linear design makes it possible to estimate partial-pixel algae coverage using a linear unmixing model. The FAI method enabled the first long-term time-series analysis of MODIS and Landsat data between 2000 and 2009 over the YS and East China Sea, revealing inter-annual variability in green tide location and size (Hu et al., 2010).

FAI and other methods have been used with remote sensing data to estimate spatial distributions and temporal changes of green tides in a number of studies (Hu et al., 2010; Keesing et al., 2011; Cui et al., 2012; Garcia et al., 2013; Xu et al., 2014; Son et al., 2015; Qi et al., 2016; Xing and Hu, 2016). Among these, each method has its own strengths and weaknesses. Some sophisticated methods such as the scaled algae index (SAI) method have been proposed (Keesing et al., 2011; Garcia et al., 2013) for image segmentation, yet they often require manual adjustments of threshold and parameterization, and such adjustments may vary among images. Therefore, FAI was chosen in this study for its simplicity, linear design (to facilitate pixel unmixing), and tolerance to perturbations by aerosols, variable solar/viewing geometry, and low to moderate sun glint (Hu, 2009). However, all these methods focused on the detection of presence/absence of *U. prolifera* and/or the area coverage of *U. prolifera*. To our knowledge, except for a limited sampling effort to determine *U. prolifera* biomass in a local region (Liu et al., 2015a; Wang et al., 2015), no study has attempted to estimate *U. prolifera* biomass at synoptic scale using either remote sensing or field measurements, due to lack of remote sensing biomass model for the former and lack of sufficient spatial/temporal coverage for the latter. On the other hand, knowledge of *U. prolifera* total biomass is essential for green macroalgae salvaging, cleaning up, and studies of carbon/nutrient cycling (Fan et al., 2014).

The primary objective of this study is therefore to develop and validate a remote sensing model to estimate *U. prolifera* biomass (wet weight and dry weight) as well as its carbon and nitrogen content. A secondary objective is to apply such a model to MODIS observations to determine the maximum total biomass in each calendar month, thus providing a reference for future mitigation efforts and ecological studies.

The structure of this manuscript is as follows. The laboratory (water tank) experiment is first introduced, with a biomass model developed and validated from independent *in situ* experiments. The model's sensitivity to variable aerosols is studied in order to apply the model to MODIS Rayleigh-corrected reflectance. The model is then applied to MODIS data between 2008 and 2015 to estimate total *U. prolifera* biomass as well as total carbon and nitrogen from daily images. Finally, the implications of these findings in model development and regional oceanography are discussed.

2. Data and method

2.1. Data collection – laboratory (water tank) experiment

In order to develop a model to convert reflectance to *U. prolifera* biomass, a water tank experiment was conducted. Fig. 2 shows the experimental setup. The water tank is 120 cm on each side and covered with black fabric to prevent light reflection from the bottom and the wall. A spectrometer (FieldSpec4, ASD Inc.) was used to measure reflectance with a 1-nm resolution between 350 and 2500 nm. A fiber-optic probe from the spectrometer was centered over the tank with a field-of-view (FOV) of 25°, which covered most of the water tank surface. The spectrometer was connected to a laptop computer to record data.

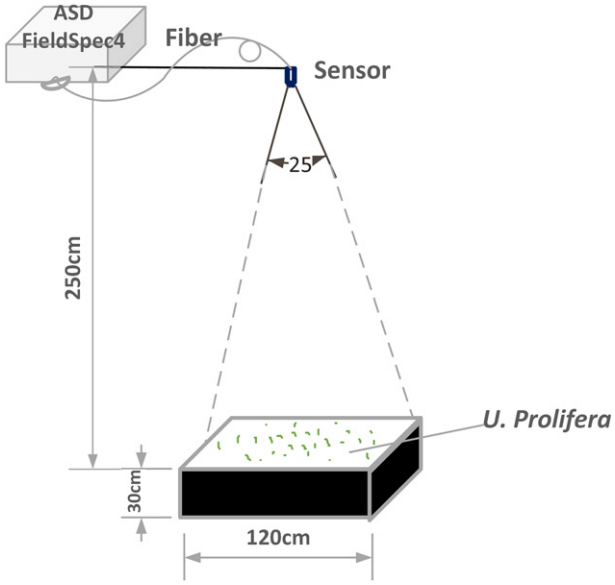

Fig. 2. Illustration of the water tank experiment to measure spectral reflectance in order to calculate FAI and determine its relationship with biomass per unit area. The set up was adjusted until the sensor's field-of-view (25°) was just within the rectangular boundary.

U. prolifera of known biomass and seawater were put in the tank to measure their reflectance. The *U. prolifera* samples were collected from coastal waters off Qingdao, whose biomasses (wet weights) were determined before they were put in the tank. To determine the biomass, the *U. prolifera* sample was put in a 2-cm mesh size net, which was then shaken manually for 3–5 min to drain excess water. Then, the wet weight of the sample was measured with a digital scale with 1 g accuracy. After putting in the water tank, biomass per area was determined as the wet weight divided by the water tank area (1.2 m × 1.2 m). Specifically, the experiment was conducted as follows: (1) Fill the water tank with seawater collected from coastal waters off Qingdao; (2) Add 0.2 kg (wet weight) *U. prolifera* in the water tank; (3) Measure reflectance of *U. prolifera* floating on the water surface ten times (reflectance was measured against a white reference plaque with a reflectance of 0.99); (4) Repeat the above steps but each time with more *U. prolifera* added until reaching a total weight of 8.0 kg. Fig. 3 shows the *U. prolifera* distribution with different biomass in the water tank. When *U. prolifera* biomass per area was increased from 0.14 kg/m^2 to 1.39 kg/m^2, the macroalgae partially covered the surface of the water tank. When the biomass reached about 2.0 kg/m^2, the surface was nearly completely covered by the macroalgae. Additional macroalgae after that did not to change the appearance in the digital photo.

The relationship between *U. prolifera* biomass and reflectance-derived FAI was used to establish a biomass remote sensing model, which was validated using *in situ* experiments described below.

2.2. Data collection – in situ experiments for model validation and carbon/nitrogen content.

In situ experiments were conducted on 11 July 2013 and 16 July 2015, respectively, in coastal waters off Qingdao. Fig. 4a shows the measurement stations, while Fig. 4b shows how *U. prolifera* was collected after reflectance was measured. *In situ* stations were selected through visual judgement of the algae density, as shown in Fig. 1. A critical requirement of the *in situ* experiment was to assure that reflectance and algae biomass were determined from the same algae patch. In practice this has been very difficult due to the movement of the boat. Therefore,

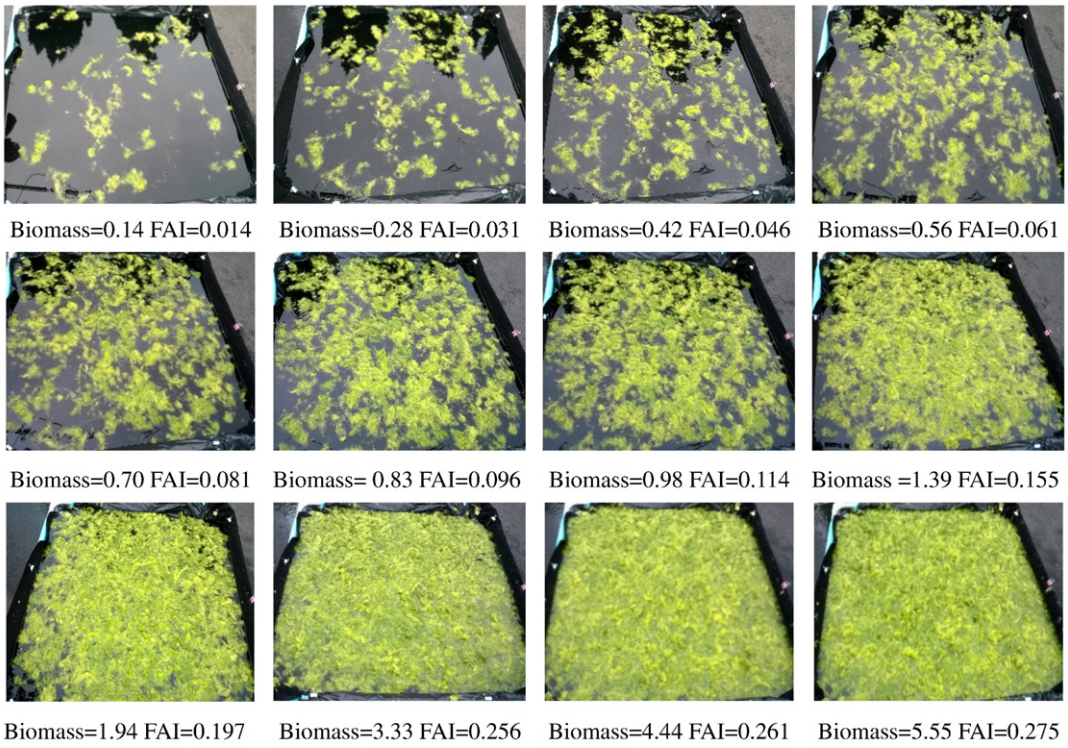

Fig. 3. Digital photos of different amount of *U. prolifera* macroalgae floating in the water tank, with their corresponding biomass per area (kg/m^2) and FAI values annotated.

such a difficulty was circumvented by conducting the two measurements in a large, relatively homogenous (in area density) algae patch at each station. From this patch, surface reflectance was first measured 10 times. Then, *U.prolifera* from the same patch was collected 3 times using laboratory-made tools. This way, because the large patch was relatively homogenous in area density, even if *U. prolifera* was collected from a slightly different location in the same patch away from the reflectance measurement, it would not cause a large mismatch between reflectance and biomass measurements. In the July 2013 experiment the tool was a steel-framed net with a 0.3 m × 0.4 m surface area. In the July 2015 experiment the tool was a fishing net with a diameter of 0.65 m (Fig. 4b). The net was carefully put underneath the algae with minimal disturbance to the algae, and then lifted to collect the algae just above its surface area. This way, the area (in m^2) from which the algae was collected was known. Such collected algae samples were placed in labelled containers, with each sample's wet weight measured with a digital scale in the laboratory after shaking off excessive waters using the procedure described in Section 2.1. Biomass per area for each sample was calculated as the wet weight divided by the surface area of the tool.

In addition to *in situ* experiments for model validation, dry weight of biomass as well as concentrations of carbon and nitrogen (per dry weight) in five *U. prolifera* samples collected on 16 July 2015 were also determined using an elemental analyzer (Vario EL III, Germany ELEMENTAR). For each sample, the wet weight of small algae pieces was determined with a high-precision (0.001 mg) scale (Germany ELEMENTAR), and then dried in a heat oven (DHG-9070A) for 24 h at 80 °C to remove water in the body of algae. The dried sample was weighed again using the same scale, and then ground to measure the carbon and nitrogen contents with the elemental analyzer. This way, for each sample, dry weight per weight wet and carbon/nitrogen concentrations (per dry weight) were determined.

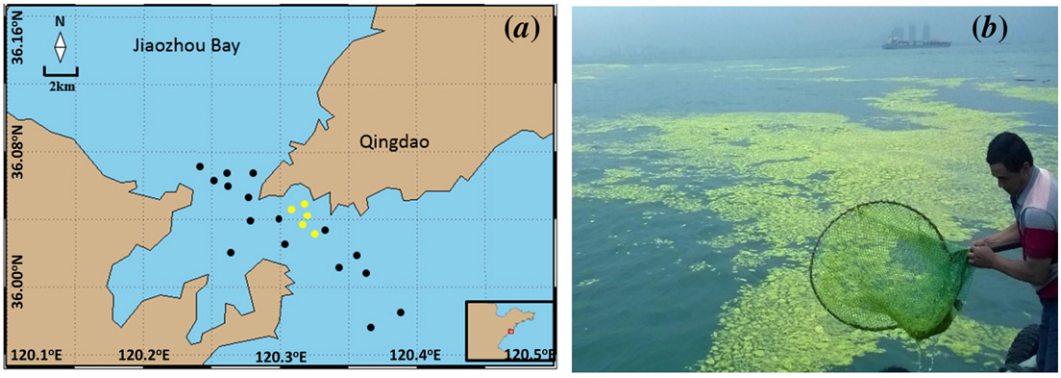

Fig. 4. (a) Stations during the field experiments on 11 July 2013 (yellow dots) and 16 July 2015 (black dots) to measure *U. prolifera* biomass per area and spectral reflectance. (b) An example of digital photos showing how *U. prolifera* was collected to determine biomass after reflectance was measured from the same *U. prolifera* patch.

2.3. Biomass model development and validation

The biomass and reflectance measurements during the laboratory experiment were used to establish a biomass remote sensing model through the reflectance-derived FAI, defined as (Hu, 2009)

$$\mathrm{FAI} = R_{\mathrm{NIR}} - R_{\mathrm{RED}} - (R_{\mathrm{SWIR}} - R_{\mathrm{RED}}) \frac{\lambda_{\mathrm{NIR}} - \lambda_{\mathrm{RED}}}{\lambda_{\mathrm{SWIR}} - \lambda_{\mathrm{RED}}} \quad (1)$$

where R is the sea surface reflectance, λ is the wavelength, the subscripts RED, NIR, and SWIR represent the red, near infrared, and shortwave infrared bands, respectively. For MODIS, $\lambda_{\mathrm{RED}} = 645$nm, $\lambda_{\mathrm{NIR}} = 859$nm, $\lambda_{\mathrm{SWIR}} = 1240$nm; For Landsat, $\lambda_{\mathrm{RED}} = 660$nm, $\lambda_{\mathrm{NIR}} = 860$-nm, $\lambda_{\mathrm{SWIR}} = 1650$nm.

In order to develop a model applicable to satellite measurements, the hyperspectral reflectance (1 nm resolution) data were first averaged for each band using the relative spectral response (RSR) functions of the satellite sensor:

$$R_{\mathrm{RED}} = \frac{\int R(\lambda) S_{\mathrm{RED}}(\lambda)}{\int S_{\mathrm{RED}}(\lambda)}, \quad (2)$$

$$R_{\mathrm{NIR}} = \frac{\int R(\lambda) S_{\mathrm{NIR}}(\lambda)}{\int S_{\mathrm{NIR}}(\lambda)},$$

$$R_{\mathrm{SWIR}} = \frac{\int R(\lambda) S_{\mathrm{SWIR}}(\lambda)}{\int S_{\mathrm{SWIR}}(\lambda)}$$

where $R(\lambda)$ is the hyperspectral reflectance, and $S(\lambda)$ is the RSR of the corresponding band, available through sensor specifications. In this study, the focus is on MODIS measurements so MODIS RSRs were used to calculate a MODIS FAI from the field-measured hyperspectral reflectance through Eqs. (1) and (2). To provide a reference for other sensors (*e.g.*, Landsat-8/OLI, NPP/VIIRS), RSRs from those sensors were also used.

Biomass per area from all laboratory measurements and their corresponding FAI values (using MODIS RSR functions) were used to establish a biomass remote sensing model through empirical regression (see Results). The model was then applied to the FAI values determined from the *in situ* measurements to estimate biomass per area, where the estimates were evaluated against the field-measured biomass per area with statistics derived to gauge the model performance.

2.4. Model application to satellite data: impacts of atmospheric effects

The biomass model was developed and validated from laboratory and field experiments. When applied to satellite data, potential impacts of the atmospheric effects must be quantified. In this study, the potential impacts were evaluated through simulations, following the approach outlined in Hu (2009).

Ideally, for each image pixel, all atmospheric effects should be estimated and removed in order to derive a surface reflectance, which can then be used as the input of the above model to estimate biomass. In practice, this is extremely difficult because the large NIR and SWIR reflectance from the *U. prolifera* makes the "black-pixel" assumption in traditional atmospheric correction approaches (Gordon and Wang, 1994; Wang and Shi, 2007; Wang et al., 2009a) no longer valid. A sophisticated approach to use the atmospheric properties derived from the algae-free pixels as surrogates for the algae-containing pixels through a "nearest-neighbor" method (Hu et al., 2000) could be developed (Shi and Wang, 2009), yet it requires pre-classification of all pixels which is still subject to errors. Therefore, instead of a full correction, a partial correction to remove the ozone absorption and Rayleigh scattering impacts was often used to derive a Rayleigh-corrected reflectance, R_{rc} (dimensionless), used as input of inversion models. The question then becomes, can the biomass model developed from the laboratory measurements be applied to MODIS R_{rc} data? If so, what are the uncertainties?

According to radiative transfer theory, R_{rc} from an algae-containing pixel can be expressed as:

$$R_{\mathrm{rc}} = R_{\mathrm{a}} + t_0 t R_{\mathrm{algae}} \quad (3)$$

where R_{a} is the reflectance due to aerosol scattering and aerosol-molecule interactions, R_{algae} is the reflectance of *U. prolifera* macroalgae floating on ocean surface (measured from *in situ* experiments), t is the atmospheric diffuse transmittance from the pixel to the sensor and t_0 is the atmospheric diffuse transmittance from the sun to the pixel.

The simulation was to determine that for each R_{algae} (and R_{algae} - derived FAI) how different combinations of R_a and $t_0\ t$ (from different aerosol types and optical thickness) may impact R_{rc} (and R_{rc} – derived FAI). In the simulation, two aerosol types were considered, with one being maritime aerosol (90% humidity, M90) and the other being coastal aerosol (50% humidity, C50). Aerosol optical thickness (AOT) at 859 nm (τ_{859}) was varied from 0.03 to 0.4, representing clear and turbid atmospheres, respectively (actually, pixels with $\tau_{859} > 0.3$ are treated as clouds in the NASA standard data processing software SeaDAS, so 0.4 represents an extreme case). For each scenario, the (R_{a},t, t_0) parameters were derived from the SeaDAS aerosol look-up tables (LUTs). Then, for each R_{algae}, R_{rc} was derived using Eq. (3), and the corresponding FAI was calculated with such derived R_{rc}, and then compared with FAI calculated from R_{algae}.

2.5. Application to MODIS time-series data

MODIS Level-0 data between April and August for each year of 2008–2015 were obtained from NASA Goddard Space Flight Center (GSFC), and then processed to generate MODIS R_{rc} data following the approach of Hu (2009). MODIS FAI was then calculated from MODIS R_{rc} for each pixel. After cloud masking, the data were mapped to a rectangular projection for the area between 33°–38°N, 118°–123°E, with each pixel representing 0.00227° (corresponding to about 250 m in the N-S direction and 205 m in the E-W direction).

The above-established biomass model was applied to each image to derive the biomass distribution. For images with minimal cloud cover, the total biomass was calculated as the integration of all biomass values from cloud-free pixels.

3. Results

3.1. Biomass and concentrations of carbon and nitrogen in U. prolifera samples

Table 1 shows the wet weight, dry weight, and concentrations of carbon and nitrogen from the five *U. prolifera* green macroalgae samples. While the wet weight was a function of sample size, the ratio between dry weight and wet weight was very stable, with the mean and standard deviation being 11.4% and 0.8%, respectively, indicating the most of the wet weight of the *U. prolifera* samples is from water. The dry/wet ratio of *U. prolifera* is actually very similar to that of *Sargassum* (a brown macroalgae, 9% ~ 12.3%) (Wong and Phang, 2004). The concentrations

Table 1
Wet weight and dry weight of each of the 5 algae samples collected in the field in 2015. Also shown are their carbon and nitrogen concentrations (weight per dry weight). In 2013 only wet weight was measured from the samples so they are not listed here.

Samples	Wet weight (mg)	Dry weight (mg)	Dry/wet (%)	Nitrogen con. (%)	Carbon con. (%)
1	20.403	2.428	11.9	1.52	29.22
2	15.640	1.564	10.0	1.33	28.45
3	15.393	1.878	12.2	1.43	28.37
4	14.241	1.652	11.6	1.24	28.81
5	14.574	1.676	11.5	1.25	28.09
Average			11.4 ± 0.8	1.35 ± 0.12	28.59 ± 0.44

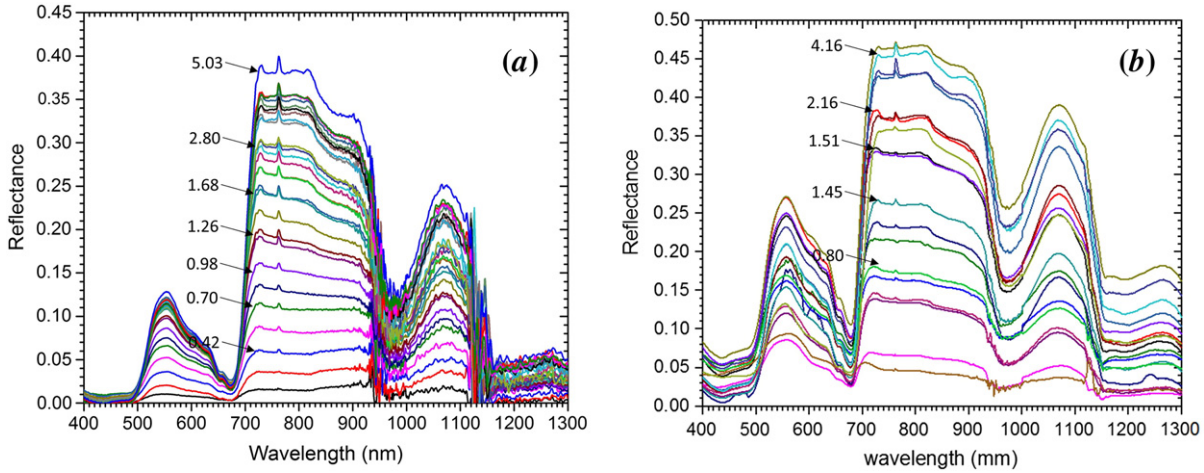

Fig. 5. (a) Reflectance spectra (dimensionless) collected from the *U. prolifera* macroalgae in the water tank experiment (Figs. 2 & 3), with total wet weight (kg/m^2) annotated for several selected spectra. (b) same as in (a) but data were collected from the *in situ* experiments (Fig. 4).

of carbon and nitrogen (per dry weight) were 28.59 ± 0.44% and 1.35 ± 0.12%, respectively. The mean C:N ratio is about 21:1, much higher than the typical Redfield ratio of 106:16 found in most phytoplankton, suggesting high carbon fixation capability by *U. prolifera*.

3.2. The biomass model, its validation, and uncertainty

Fig. 5a and b show the reflectance spectra of *U. prolifera* measured from the laboratory and *in situ* experiments, respectively, where their corresponding biomass (wet weight) per area are annotated for some representative spectra. From visual inspection, the NIR reflectance increased sharply with increasing biomass when concentration was <~2 kg/m^2. Beyond this concentration, the NIR reflectance appeared to be saturated with further increased biomass and it increased at a much slower pace, indicating that algae aggregates more in the vertical direction rather than in the horizontal direction. This observation is consistent from the visual appearance of the algae photos shown in Fig. 3.

Fig. 6 shows the relationship between FAI (calculated from surface hyperspectral reflectance weighted by the MODIS RSR function using Eqs. (1) and (2)) and biomass per area from both laboratory and *in situ* experiments, confirming the above visual inspection. Here biomass ranged from 0.14 to 5.55 kg/m^2 (N = 28) from the laboratory experiment and from 0.42 to 4.22 kg/m^2 (N = 21) from the *in situ* experiments. Overall, FAI is a monotonic function of biomass, where the latter can be derived from the former. Specifically, three findings could be derived from the figure.

First, for FAI < 0.2, a linear, stable relationship was found between FAI and biomass. Above this threshold, FAI appears to be saturated with further increases in biomass and the relationship appears non-linear, with rapid increases in biomass following increases in FAI.

Second, for FAI < 0.2, the FAI-biomass relationship appeared to be stable between laboratory and *in situ* measurements, suggesting that a robust model could be developed to estimate biomass from FAI. Above this threshold, laboratory and *in situ* experiments showed different FAI-biomass relationship.

Third, in general, *in situ* measurements showed much higher uncertainties (in both FAI and biomass) than laboratory measurements, as shown by the higher standard deviations from the former (5.9% for FAI and 12.4% for biomass in contrast to 1% from the latter). This is apparently due to the difficulty in conducting accurate measurements of the moving *U. prolifera* patch from a small boat. However, both types of measurements showed nice agreement for FAI < 0.2.

Because of the lower uncertainties, the data from the laboratory experiments (filled triangles in Fig. 6) were used to develop an empirical model to estimate biomass per area from FAI. A step-wise least-square fitting was used to develop the model, expressed as

$$\begin{cases} y = 9x + 0.014 & -0.0015 < x \le 0.2 \\ y = e^{18.1(x-0.2)} + 0.814 & 0.2 < x \le 0.3 \end{cases} \quad (4)$$

where x is FAI (dimensionless) and y is the *U. prolifera* biomass per area in kg/m^2.

The model in Eq. (4) was evaluated using *in situ* data in Fig. 7a, which shows the *in situ* biomass per area in the x-axis and modelled biomass (from *in situ* reflectance) per area in the y-axis. For biomass < 2 kg/m^2 (corresponding to FAI ~ 0.2), relative uncertainties are about 14–16% with no bias. Here relative uncertainties were estimated as either relative Root-Mean-Square Difference (RMSD) or absolute Mean Relative Difference (MRD), and bias was estimated as the Mean Ratio (MR). For biomass > 2 kg/m^2, not only did relative uncertainties increase to ~40%, but bias also increased to 40% (MR = 1.4), suggesting larger errors when the algae density becomes higher.

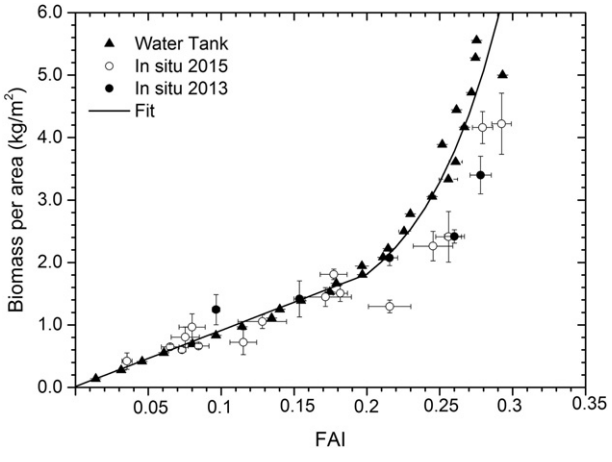

Fig. 6. Scatter plot showing the relationship between *U. prolifera* macroalgae biomass per area and FAI determined from surface reflectance. Filled triangles represent data collected from the water tank experiment, with the solid line represents the best fit through least-square fitting. Filled and empty circles represent data collected from the field experiments on 11 July 2013 and 16 July 2015, respectively. The horizontal bars are the standard deviations of FAI values from 10 reflectance measurements, and the vertical bars are the standard deviations of 3 wet weight measurements. Note that because for remote sensing applications FAI is the independent variable and biomass is the dependent variable, the x-axis and y-axis as well as the model in Eq. (4) are arranged accordingly.

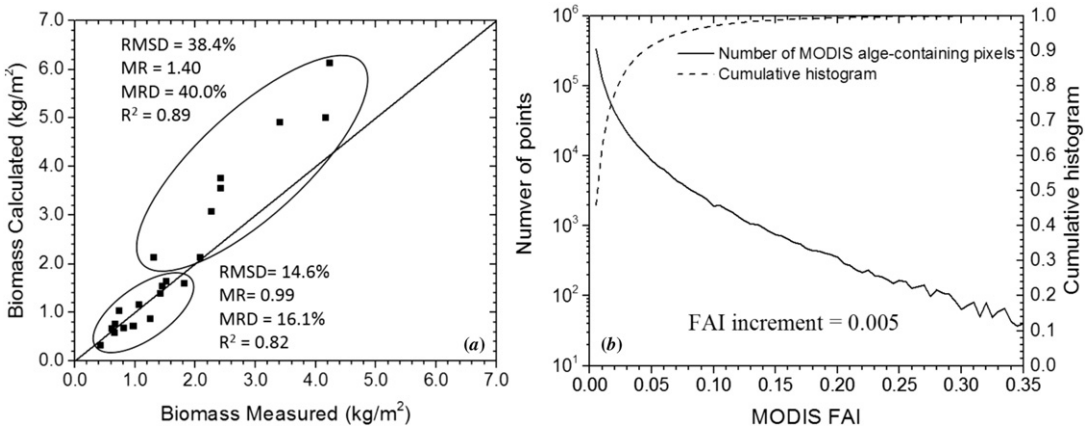

Fig. 7. (a) Validation of laboratory based biomass-FAI model (Eq. (4)) using field measurements. Note that below 2 kg/m^2 (corresponding to FAI = 0.2) the model is more accurate than above 2 kg/m^2; (b) For MODIS imagery, 99.5% of algae-containing pixels from 12 cloud-free MODIS images in summer 2015 have FAI < 0.2, suggesting that the model is accurate for nearly all pixels.

However, in practice such increased uncertainties at high FAI values will have negligible impact on estimating either biomass distribution or total biomass. This is because very few algae-containing pixels will have FAI > 0.2. Fig. 7b shows the histogram and cumulative histogram of FAI values derived from 12 cloud-free MODIS images during summer 2015. Only algae-containing pixels were used in the statistics. Clearly, >99.5% of the algae-containing pixels have FAI values < 0.2. Therefore, for nearly all pixels, the validation results obtained in Fig. 7a for FAI < 0.2 should be applicable. For this reason, the upper bound FAI value corresponding to 100% algae coverage within a pixel was regarded to be 0.2. If a MODIS pixel had FAI > 0.2 (this is very rare according to Fig. 7b), the second part of Eq. (4) was applied. In the end, because the biomass of a pixel was determined using its own FAI value through Fig. 6 and Eq. (4), the selection of the upper bound value had no impact on biomass estimates for either individual pixels or the entire image.

The simulation results by adding aerosol impacts (Eq. (3)) further indicated that the model in Eq. (4), although derived from laboratory measurements, may be applied directly to MODIS R_{rc} data with small uncertainties. Fig. 8a shows one example of the simulated MODIS FAI against field-measured FAI under variable aerosol optical thickness $\tau_a(859)$ and aerosol types when field-measured FAI was 0.216. Clearly, the simulated MODIS FAI decreased with increasing $\tau_a(859)$ for both aerosol types but with different changing rate. In both cases, however, changes in the simulated MODIS were < 10% even between the two extreme AOT cases. Fig. 8b further shows the mean and standard deviation of simulated MODIS FAI against the *in situ* FAI under different environmental conditions. Although small departures from the 1:1 line were found, the agreement between the two was excellent. Under all simulated conditions in this study, the average and maximum relative errors in the simulated MODIS FAI values, as gauged by the corresponding *in situ* FAI values, were 6.5% and 12.3%, respectively. Considering the patchiness of *U. prolifera* mats in the field, such small uncertainties should be regarded as acceptable, and the biomass model in Eq. (4) can therefore be applied directly to MODIS R_{rc} data to derive biomass distributions and total biomass from individual images.

3.3. MODIS-derived biomass distributions

U. prolifera often appeared in MODIS FAI imagery as small image slicks in Subei Shoal at the end of April, which were advected northward, forming a massive bloom in the YS during June and July. The biomass images showed the same temporal and spatial changes as from the FAI images, yet the biomass images provided additional information on the *U. prolifera* abundance at each location. Fig. 9 shows two examples on 25 June 2008 and 21 June 2015, where biomass per area is color coded for each pixel. Most of the algae-containing pixels contained very low density of algae (<0.3 kg/m^2), while a small portion of the pixels showed moderate densities around 0.4–0.5 kg/m^2. The total algae amount in June 2015 appeared to be much higher than in June

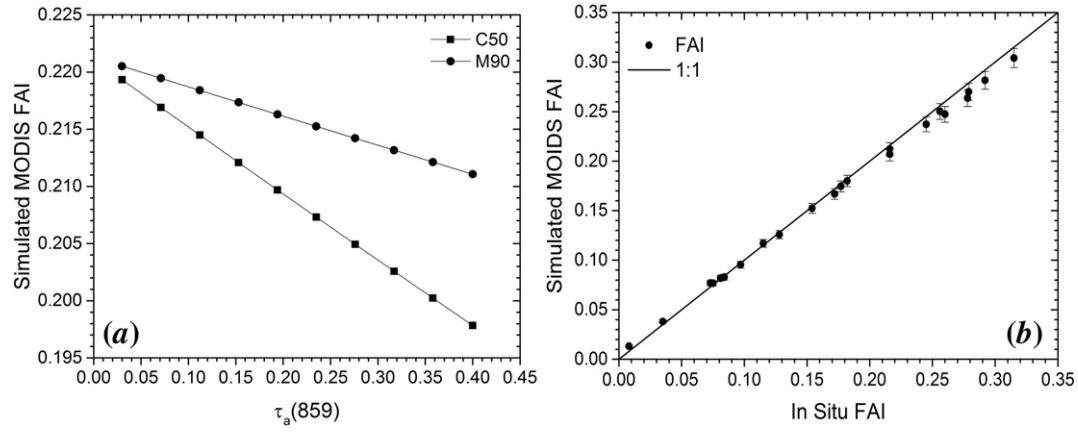

Fig. 8. (a) Simulated MODIS FAI as a function of aerosol optical thickness at 859 nm ($\tau_a(859)$, dimensionless) for maritime and coastal aerosol types when the field-measured FAI is 0.216. Note that when $\tau_a(859)$ is >0.3, atmosphere is regarded being very turbid and ocean color retrievals are impossible in the standard NASA processing (*i.e.*, the pixels are masked without being further processed). Mean $\tau_a(859)$ for the study region (determined from NASA global data) is about 0.16. (b) Relationship between simulated MODIS FAI and field FAI for all aerosol types and optical thickness used in the simulation.

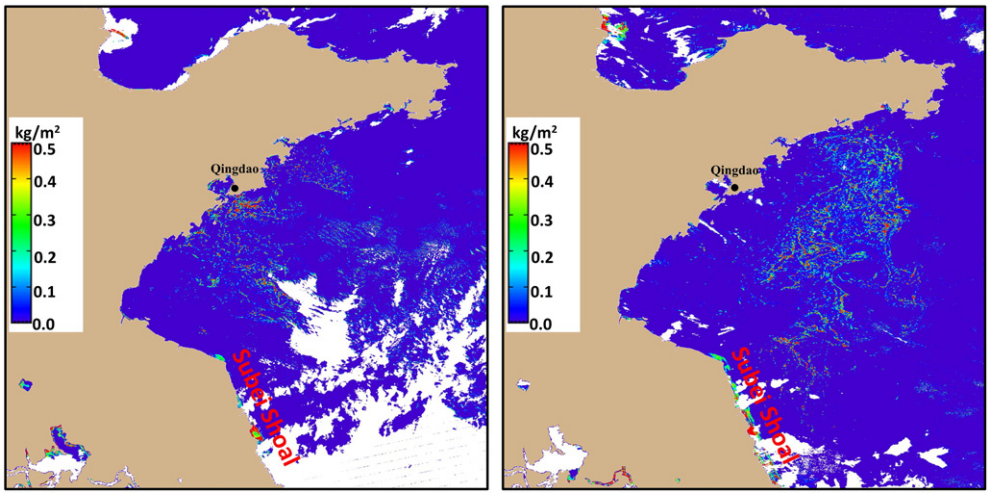

Fig. 9. Distributions of *U. prolifera* biomass (wet weight) per area derived from MODIS on 25 June 2008 (left) and 21 June 2015 (right), respectively. White color represents clouds, and the green-reddish colors along the Subei Shoal are image artifacts due to extremely shallow bathymetry. The location of Qingdao is annotated with a black dot.

2008, yet most algae appeared near Qingdao in June 2008, explaining the world-renowned green tide event that year.

Such an observation is reinforced by the 2008–2015 time series of MODIS observations, shown in Fig. 10. Although due to frequent cloud cover the time series was not continuous in time, the seasonal patterns and inter-annual changes can still be clearly visualized. These patterns agree well with those reported earlier, but with absolute total biomass reported here. While each year showed similar temporal pattern where *U. prolifera* biomass started to increase around day 140 and peaked around day 170–180, significant inter-annual variability was observed in the algae biomass, with the amount in 2015 at least doubled those in other years for the peak months.

The total biomass, total carton, and total nitrogen contained in *U. prolifera* on 8 maximum days between 2008 and 2015 are presented in Table 2. The year of 2012 represented the minimal green tide year while the year of 2015 was the maximum green tide year, with the total algae biomass in the latter 20 times higher than in the former. The factors leading to such extreme inter-annual variability, however, are yet to be studied.

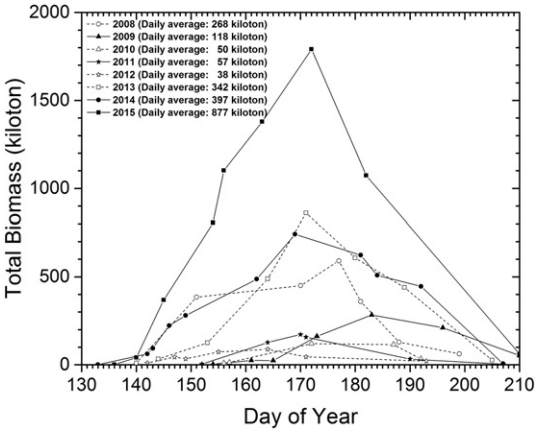

Fig. 10. Total *U. prolifera* biomass (wet weight) in the YS derived from individual MODIS images using the biomass model in Eq. (4) in relatively cloud-free days of each spring-summer between 2008 and 2015. Each point represents total biomass corresponding to the MODIS measurement time. The annotated number for each year represents the mean daily biomass between day 140 and day 210. To account for uneven temporal gaps due to cloud cover, the mean was not calculated as a simple average of the cloud-free days, but calculated as an integration of cloud-free days divided by the temporal interval (*i.e.*, the area covered by each curve divided by 70).

4. Discussion

4.1. Uncertainties in biomass estimates

Ideally, satellite-based estimates required field validation in order to assess uncertainties. However, in the case of *U. prolifera*, it is impossible to carry out such a direct validation and uncertainty assessment. This is simply because that 1) *U. prolifera* is very patchy and its coverage is often much smaller than a MODIS 250-m pixel; 2) technically it is nearly impossible to collect all *U. prolifera* within just a MODIS pixel precisely; 3) the typical 0.5-pixel image registration error also makes it impossible to find the exact area on the water surface corresponding to a MODIS pixel. The difficulty in such a direct validation represents the most limiting factor for the biomass model developed here, but it is an inherent problem for any models that attempt to estimate coverage or area density of any floating materials in the ocean.

However, this does not mean that uncertainties cannot be evaluated from the biomass estimates. The assessment of the laboratory-based model using independent *in situ* data clearly showed model robustness with small (14–16%) uncertainties for nearly all MODIS pixels (Fig. 7). The aerosol simulations further showed additional uncertainties of ~6.5% (maximum 12.3%) when applied to MODIS R_{rc} data (Fig. 8). Thus, even in the worst case scenario, the total uncertainties would be

Table 2
Statistics of *U. prolifera* in the YS between 2008 and 2015. The first three columns show maximum daily total wet biomass, carbon, and nitrogen during every year between 2008 and 2015 estimated from MODIS data using the biomass model developed in this study. Also listed is the average daily growth rate calculated from multiple images. The last column shows cumulative wet weight biomass of *U. prolifera* collected by local agency during each year.

Year	Total wet biomass (kiloton)	Total carbon (kiloton)	Total nitrogen (kiloton)	Average growth rate (% per day)	Annual cumulative wet biomass collected by local agency[a] (kiloton)
2008	591	19.26	0.91	11.6	76
2009	283	9.22	0.44	15.8	
2010	120	3.91	0.18	17.5	32
2011	172	5.61	0.26	23.1	10
2012	88	2.87	0.14	16.5	12
2013	860	28.03	1.32	12.8	185
2014	742	24.18	1.14	9.7	101
2015	1791	58.37	2.76	12.5	265

[a] Data from "Report on Marine Environmental Quality of Qingdao" between 2008 and 2015. Because some local group may have not reported algae collection and nearly all these collection were from nearshore waters, these are provided here as a reference only, and they represent the lower bounds from the mitigation efforts.

the mean square root of 16% and 12.3% = 20% for most pixels. Considering that 35% was generally accepted as a standard for uncertainties in chlorophyll retrievals at pixel level, 20% in the derived biomass should be acceptable. On the other hand, these estimates are for *U. prolifera* in offshore waters. For inshore waters near beaches, shorelines, or large marine facilities, *U. prolifera* may aggregate and become thicker than in offshore waters, resulting in FAI > 0.2 (last three panels in Fig. 3). Under these circumstances, *U. prolifera* biomass will be underestimated by ~40% for local regions (Fig. 7a). However, MODIS statistics in Fig. 7b suggest that such circumstances are rare (<0.5%), therefore, not indicating a significant shortcoming of the biomass model. In addition, the seasonality in every year and inter-annual variation patterns shown in Fig. 10 are all consistent with those reported in the published literature (Xu et al., 2014; Qi et al., 2016), thus providing an extra validity check. Note that these annual variations are not due to changes in cloud covers because only cloud-free days were used in the MODIS estimates.

One may wonder whether the physically collected biomass, shown in the last column of Table 2, could be used to partially validate the MODIS-based biomass estimates. While in theory if the exact information on the physical collection, such as the area and time interval of the collection, were known, these numbers could provide a direct validation of the MODIS estimates for the same area and time interval. Unfortunately this is not the case. Instead, the physical collection was mostly restricted to nearshore waters and those washed on the beaches, which missed algae in offshore waters where most algae were found. The exact collection times were not known either. In addition, not every group reported their collection to the official agency in charge of management and reports. Therefore, the reported values of biomass collection in Table 2 represent only a small and also possibly disproportional portion of the total algae amount floating on the sea surface as estimated from MODIS, yet they can still provide useful information for a partial, relative validation. For example, the relatively low-biomass MODIS years (2010 − 2012) also showed low collection amount as compared with other years. Furthermore, excluding those low-biomass years of 2010–2012 where algae collection could be significantly disproportional to the total daily maximum amount, all other years showed very close ratios (6.6 ± 1.4, coefficient of variance = 21%) between the two, suggesting a partial validation

4.2. Implications for mitigation and other studies

Each year, in order to maintain a clean environment to attract tourism, local governmental agencies spent enormous amount of resources to collect *U. prolifera* accumulated on both beaches and ocean surface. Table 2 shows the total collected algae biomass (wet weight) during each year reported by one agency. Considering that the algae weight often contained sand particles from beaches and water from boat operations, perhaps only 50% of these weight numbers are from pure algae. Then, compared with the daily maximum amount in Table 2, only 3–13% of the total biomass from a single day (the maximum day) was physically removed. Note that the total biomass estimated from MODIS was from a single day without any consideration of the algae growth. In reality, the cumulated algae biomass over the period of April–July could only be higher than the single-day estimates. Clearly, physical removal only accounted for a very small portion of the total *U. prolifera* biomass. Even when considering that the actual amount from the mitigation could be higher than those listed in Table 2 because some groups may have chosen not to report, the "missing" values may still be comparable to those reported values. However, given the fact that most *U. prolifera* never landed but rather dissipated naturally in the ocean, the physical removal may be an effective mitigation method to keep a clean environment around the beaches.

Mitigation efforts require timely information on *U. prolifera* location and amount. In the past, a web-based green tide online monitoring system (ORSIFAI) was established using the FAI method and multi-sensor satellite data (He et al., 2011; ORSIFAI, 2009). The system produces and shares Red-Green-Blue composite images, FAI images, green tide thematic maps, as well as environmental variables such as sea surface temperature (SST), chlorophyll-a concentration (Chla), photosynthetically active radiation (PAR), and sea surface wind (SSW). The system has been running since 2009 as a prototype early-warning system to alert the local government for possible mitigation effort. However, the system only showed presence/absence of *U. prolifera* at certain locations. With the biomass model developed from this study and applied to MODIS, the monitoring system will be able to provide quantitative estimate of *U. prolifera* biomass at any cloud-free location, thus helping to make mitigation and other management decisions. The biomass information near beaches may be particularly useful as it can help the management agencies to estimate how much resource (number of boats and personnel) is required for mitigation.

U. prolifera growth rate has been determined in the past from field culturing experiments. Here, during the first half of the bloom cycle when *U. prolifera* started to appear in MODIS imagery and then reached the daily maximum, daily growth rate (α, d^{-1}) was estimated as $B_{d\_n} = B_{d\_1}(1+\alpha)^n$, where d_1 is for day 1, day_n is for day n, n is the number of days between the two MODIS observations, and B is integrated biomass. The average daily growth rate for each year is listed in Table 2. For all years, the average is 15 ± 4% d^{-1}. This is lower than the reported value based on experiments over field cultures under controlled conditions (23–26%) (Zhang et al., 2013; Wang et al., 2015). One possible reason for the difference is that the "growth rate" estimated from MODIS included algae mortality. The annual variations in such calculated growth rate may result from changes in growth conditions, which needs to be verified from more field experiments. On the other hand, these MODIS-determined growth rates may be used in ecological models to model the bloom's evolution in time and how the bloom responds to other environmental forcing.

To date, very few studies reported primary production or carbon fixation of *U. prolifera* in the YS. The MODIS determined carbon and nitrogen contents from daily imagery in Table 2 may provide some constraints to refine primary production models. They may also be combined with carbon fixation data determined from field measurements (Liu et al., 2015b; Song et al., 2008) to provide a better context for carbon studies.

4.3. Application to other satellite sensors

The model developed in this study is for MODIS FAI data. Actually nearly all satellite sensors with the appropriate spectral bands can be used for monitoring green tides. Some of these sensors have similar RED, NIR, and SWIR bands to enable the derivation of sensor-specific FAI. These include Landsat-8/OLI, sentinel-2/MSI, NPP/VIIRS, and FY-3A&B/MERSI. However, their band widths and band centers differ from those of MODIS, thus requiring some adjustments of the model coefficients. Specifically, the upper bound of FAI for 100% *U. prolifera* coverage needs to be determined from each sensor. This has been achieved through simulations using the hyperspectral reflectance corresponding to 100% *U. prolifera* (*i.e.*, MODIS FAI = 0.216), the relative spectral response function of each sensor, and same radiative transfer simulations to take account of variable aerosols when satellite-derived R_{rc} data are used. The simulated FAI numbers for the various sensors were scaled to MODIS FAI of 0.2 with the corresponding biomass of 2.0 kg/m^2. The results are listed in Table 3. Because a longer SWIR band was used (*i.e.*, 1.6 um *versus* MODIS 1.2 um), FAI from these sensors is higher than the corresponding MODIS FAI. The difference reaches 14% for the MSI sensor. Considering the 20% uncertainties from the model and variable aerosols, the total uncertainties would reach 25% when the MODIS model developed here were to be applied to these sensors even in the worst-case scenarios. Considering the complex situations of measuring these patchy macroalgae, even this 25% uncertainty may still be acceptable.

Table 3
FAI values (last column) of Landsat-8/OLI, Sentinel-2/MSI, NPP/VIIRS, and FY3/MERSI corresponding to the field-measured MODIS FAI of 0.2 (*i.e.*, 2 kg m^{-2} *U. prolifera* coverage on the surface). These can be used to represent the upper bounds (*i.e.*, 100%) *U. prolifera* coverage for the individual sensors when their satellite-derived FAI data are used to estimate biomass. The lower bounds for the individual sensors need to be determined from their corresponding images. The upper bound and lower bound for an individual sensor can then be used to estimate biomass per pixel following the same approach of Qi et al. (2016). For completeness the 3 bands used for the FAI calculation and the spatial resolution for each sensor are also listed.

Satellite/sensor	λ_{RED} (um)	λ_{NIR} (um)	λ_{SWIR} (um)	Spatial resolution (m)	FAI
Landsat-8/OLI	0.63–0.68	0.845–0.885	1.56–1.66	30	0.216 ± 0.007
Sentinel-2/MSI	0.65–0.68	0.855–0.875	1.565–1.655	20	0.228 ± 0.007
NPP/VIIRS	0.60–0.68	0.85–0.88	1.58–1.64	375	0.200 ± 0.006
FY3/MERSI	0.635–0.675	0.84–0.88	1.615–1.665	250	0.211 ± 0.007

4.4. Implications for monitoring Sargassum blooms

Since 2011, blooms of the brown macroalgae *Sargassum spp.* (mostly *S. fluitans* and *S. natans*) occurred every year in the Caribbean (Wang and Hu, 2016). Although *Sargassum* is a critical habitat for fish and other marine animals, significant *Sargassum* beaching can cause similar environmental and economical problems as *U. prolifera* beaching in Qingdao (Hu et al., 2016). Due to lack of direct biomass measurements, Wang and Hu (2016) could only use a density estimate (in % cover) to describe *Sargassum* abundance and its spatial and temporal distributions. The approach developed here to estimate *U. prolifera* biomass can be easily transferred to *Sargassum* measurements. Indeed, once *Sargassum* biomass per area is determined from a pure (100% coverage) *Sargassum* mat, the number can be applied to all results obtained in Wang and Hu (2016) to convert the percent coverage to absolute total biomass. Such an experiment may be conducted in the near future in order to provide a more quantitative estimate of *Sargassum* blooms.

5. Conclusion

Remote sensing studies of *U. prolifera* green tides in the YS are not new, but to date it has been impossible to estimate *U. prolifera* biomass, not to mention its carbon and nitrogen content. This knowledge gap is now filled by the current study through carefully designed experiments, radiative transfer simulations, and a validated biomass model. All results showed the model robustness with known uncertainties, leading to application of the model to MODIS imagery to derive biomass distributions.

The findings will have direct impact on future mitigation efforts as quantitative biomass estimates will now be available in near real-time through an existing monitoring system. The findings also have significant implications for monitoring blooms of other macroalgae such as *Sargassum* spp. in the Intra-Americas Sea, as the model development approach may be extended to develop models for other macroalgae.

Acknowledgements

This work was supported by the Qingdao Science and Technology Project (No. 14-9-3-2-HY), National Basic Research Program of China (No. 2012CB957704) and National Natural Science Foundation of China (Nos. 60638020 and 61675187). We thank the Laboratory of Phycology and Algal Aquaculture of Ocean University of China (OUC) for measuring carbon and nitrogen concentrations from algae samples, and thank NASA MODIS team for providing MODIS data. We thank Prof. Fumin Guan from OUC for providing valuable comments about field experiment. We also thank Dr. Jianjun Liang, Ms. Xiaoyan Liu, Mr. Zhongwei Huang, and Ms. Bingqing Huang for their help in the laboratory and *in situ* experiment. Three anonymous provided valuable comments to help improve the presentation of this manuscript, whose efforts are greatly appreciated.

References

Charlier, R.H., Morand, P., Finkl, C.W., Thys, A., 2006. Green tides on the Brittany coasts. 2006 IEEE US/EU Baltic International Symposium:pp. 1–13 http://dx.doi.org/10.1109/BALTIC.2006.7266128.

China Marine Disaster Bulletin, 2008–2013. State Oceanic Administration People's Republic of China. http://www.soa.gov.cn/zwgk/hygb/zghyzhgb/.

Cui, T., Zhang, J., Sun, L., Jia, Y., Zhao, W., Wang, Z., Meng, J., 2012. Satellite monitoring of massive green macroalgae bloom (GMB): imaging ability comparison of multi-source data and drifting velocity estimation. Int. J. Remote Sens. 33, 5513–5527.

Fan, X., Xu, D., Wang, Y., Zhang, X., Cao, S., Mou, S., Ye, N., 2014. The effect of nutrient concentrations, nutrient ratios and temperature on photosynthesis and nutrient uptake by *Ulva prolifera*: implications for the explosion in green tides. J. Appl. Phycol. 26, 537–544.

Garcia, R.A., Fearns, P., Keesing, J.K., Liu, D., 2013. Quantification of floating macroalgae blooms using the scaled algae index. J. Geophys. Res. Oceans 118, 26–42.

Gordon, H.R., Wang, M., 1994. Retrieval of water-leaving radiance and aerosol optical thickness over the oceans with SeaWiFS: a preliminary algorithm. Appl. Opt. 33, 443–452.

Gower, J., Hu, C., Borstad, G., King, S., 2006. Ocean color satellites show extensive lines of floating Sargassum in the Gulf of Mexico. IEEE Trans. Geosci. Remote Sens. 44, 3619–3625.

He, M.-X., Liu, J., Yu, F., Li, D., Hu, C., 2011. Monitoring green tides in Chinese marginal seas. In: Jesus Morales, V.S., Platt, Trevor, Sathyendranath, Shubha (Eds.), Handbook of Satellite Remote Sensing Image Interpretation: Applications for Marine Living Resources Conservation and Management. EU PRESPO and IOCCG, Dartmouth, Canada, pp. 111–124.

Hu, C., 2009. A novel ocean color index to detect floating algae in the global oceans. Remote Sens. Environ. 113, 2118–2129.

Hu, C., Carder, K.L., Muller-Karger, F.E., 2000. Atmospheric correction of SeaWiFS imagery over turbid coastal waters: a practical method. Remote Sens. Environ. 74, 195–206.

Hu, C., He, M.-X., 2008. Origin and offshore extent of floating algae in olympic sailing area. EOS Trans. Am. Geophys. Union 89, 302–303.

Hu, C., Li, D., Chen, C., Ge, J., Muller-Karger, F.E., Liu, J., Yu, F., He, M.-X., 2010. On the recurrent *Ulva prolifera* blooms in the Yellow Sea and East China Sea. J. Geophys. Res. 115, C0501.

Hu, C., Murch, B., Barnes, B.B., Wang, M., Maréchal, J.-P., Franks, J., Lapointe, B.E., Goodwin, D.S., Schell, J.M., Siuda, A.N., 2016. Sargassum watch warns of incoming seaweed. EOS Trans. Am. Geophys. Union 97 (22), 10–15.

Keesing, J.K., Liu, D., Fearns, P., Garcia, R., 2011. Inter- and intra-annual patterns of *Ulva prolifera* green tides in the Yellow Sea during 2007–2009, their origin and relationship to the expansion of coastal seaweed aquaculture in China. Mar. Pollut. Bull. 62, 1169–1182.

Lü, X., Qiao, F., 2008. Distribution of sunken macroalgae against the background of tidal circulation in the coastal waters of Qingdao, China, in summer 2008. Geophys. Res. Lett. 35, L23614. http://dx.doi.org/10.1029/2008GL036084.

Leliaert, F., Zhang, X., Ye, N., Malta, E.-j., Engelen, A.H., Mineur, F., Verbruggen, H., De Clerck, O., 2009. Research note: identity of the Qingdao algal bloom. Phycol. Res. 57, 147–151.

Liang, Z., Lin, Z., Ma, M., Zhang, J., Yan, X., Liu, T., 2008. A preliminary study of the *Enteromorpha prolifera* drift gathering causing the green tide phenomenon. (In Chinese with English Abstract). J. Ocean Univ. China 38, 601–604.

Liu, D., Keesing, J.K., Xing, Q., Shi, P., 2009. World's largest macroalgal bloom caused by expansion of seaweed aquaculture in China. Mar. Pollut. Bull. 58, 888–895.

Liu, D., Keesing, J.K., Dong, Z., Zhen, Y., Di, B., Shi, Y., Fearns, P., Shi, P., 2010. Recurrence of the world's largest green-tide in 2009 in Yellow Sea, China: *Porphyra yezoensis* aquaculture rafts confirmed as nursery for macroalgal blooms. Mar. Pollut. Bull. 60, 1423–1432.

Liu, D., Keesing, J.K., He, P., Wang, Z., Shi, Y., Wang, Y., 2013a. The world's largest macroalgal bloom in the Yellow Sea, China: formation and implications. Estuar. Coast. Shelf Sci. 129, 2–10.

Liu, F., Pang, S., Chopin, T., Gao, S., Shan, T., Zhao, X., Li, J., 2013b. Understanding the recurrent large-scale green tide in the Yellow Sea: temporal and spatial correlations between multiple geographical, aquacultural and biological factors. Mar. Environ. Res. 83, 38–47.

Liu, X., Li, Y., Wang, Z., Zhang, Q., Cai, X., 2015a. Cruise observation of *Ulva prolifera* bloom in the southern Yellow Sea, China. Estuar. Coast. Shelf Sci. 163 (Part A), 17–22.

Liu, J., Yu, Z., Zang, J., Sun, T., Zhao, C., Ran, X., 2015b. Distribution and budget of organic carbon in the Bohai and Yellow Seas. (in Chinese). Adv. Earth Sci. 30, 564–578.

Mail Daily, 2008. http://www.dailymail.co.uk/news/article-1031444/Chinas-blooming-algae-problem-thats-swamping-Olympics.html.

Nelson, T.A., N., A.V., Tjoelker, M., 2003. Seasonal and spatial patterns of "green tides" (ulvoid algal blooms) and related water quality parameters in the coastal waters of Washington State, USA. Bot. Mar. 46, 263–275.

ORSIFAI, 2009. http://115.28.50.80:8080/algae.

Pang, S.J., Liu, F., Shan, T.F., Xu, N., Zhang, Z.H., Gao, S.Q., Chopin, T., Sun, S., 2010. Tracking the algal origin of the Ulva bloom in the Yellow Sea by a combination of molecular, morphological and physiological analyses. Mar. Environ. Res. 69, 207–215.

Qi, L., Hu, C., Xing, Q., Shang, S., 2016. Long-term trend of *Ulva prolifera* blooms in the western Yellow Sea. Harmful Algae 58, 35–44.
Qiao, F., Wang, G., Lü, X., Dai, D., 2011. Drift characteristics of green macroalgae in the Yellow Sea in 2008 and 2010. Chin. Sci. Bull. 56, 2236–2242.
Qingdao News, 2008. http://qdsq.qingdao.gov.cn/n15752132/n15752817/n26276611/n26378128/n26387592/n26388048/26422826.html.
Shen, Q., Li, H., Li, Y., Wang, Z., Liu, J., Yang, W., 2012. Molecular identification of green algae from the rafts based infrastructure of *Porphyra yezoensis*. Mar. Pollut. Bull. 64, 2077–2082.
Shi, W., Wang, M., 2009. Green macroalgae blooms in the Yellow Sea during the spring and summer of 2008. J. Geophys. Res. Oceans 114, C12010. http://dx.doi.org/10.1029/2009JC005513.
Son, Y.B., Choi, B.-J., Kim, Y.H., Park, Y.-G., 2015. Tracing floating green algae blooms in the Yellow Sea and the East China Sea using GOCI satellite data and Lagrangian transport simulations. Remote Sens. Environ. 156, 21–33.
Song, J., Li, X., Yuan, H., Zheng, G., Yang, Y., 2008. Carbon fixed by phytoplanton and cultured algae in China coastal seas. (in Chinese). Acta Ecol. Sin. 28, 551–558.
Taylor, R., Fletcher, R.L., Raven, J.A., 2001. Preliminary studies on the growth of selected green-tide algae in laboratory culture effects of irradiance, temperature, salinity and nutrients on growth rate. Bot. Mar. 44, 327–336.
Wang, M., Hu, C., 2016. Mapping and quantifying Sargassum distribution and coverage in the Central West Atlantic using MODIS observations. Remote Sens. Environ. 183, 350–367.
Wang, M., Shi, W., 2007. The NIR-SWIR combined atmospheric correction approach for MODIS ocean color data processing. Opt. Express 15, 15,722–15,733.
Wang, M., Son, S., Shi, W., 2009a. Evaluation of MODIS SWIR and NIR-SWIR atmospheric correction algorithms using SeaBASS data. Remote Sens. Environ. 113, 635–644.
Wang, X.H., Li, L., Bao, X., Zhao, L.D., 2009b. Economic cost of an algae bloom cleanup in China's 2008 Olympic Sailing Venue. EOS Trans. Am. Geophys. Union 90, 238–239.
Wang, Z., Xiao, J., Fan, S., Li, Y., Liu, X., Liu, D., 2015. Who made the world's largest green tide in China?—an integrated study on the initiation and early development of the green tide in Yellow Sea. Limnol. Oceanogr.:1–21 http://dx.doi.org/10.1002/lno.10083.
Wong, C., Phang, S., 2004. Biomass production of two Sargassum species at Cape Rachado, Malaysia. Hydrobiologia 512, 79–88.
Xing, Q., Hu, C., 2016. Mapping macroalgal blooms in the Yellow Sea and East China Sea using HJ-1 and Landsat data: application of a virtual baseline reflectance height technique. Remote Sens. Environ. 178, 113–126.
Xu, Q., Zhang, H., Cheng, Y., Zhang, S., Zhang, W., 2016. Monitoring and tracking the green tide in the Yellow Sea with satellite imagery and trajectory model. IEEE J. Sel. Top. Appl. Earth Obs. Remote Sens. 9 (11), 5172–5181.
Xu, Q., Zhang, H., Ju, L., Chen, M., 2014. Interannual variability of *Ulva prolifera* blooms in the Yellow Sea. Int. J. Remote Sens. 35, 4099–4113.
Yabe, T., Ishii, Y., Amano, Y., Koga, T., Hayashi, S., Nohara, S., Tatsumoto, H., 2009. Green tide formed by free-floating Ulva spp. at Yatsu tidal flat, Japan. Limnology 10, 239–245.
Ye, N., Zhang, X., Mao, Y., Liang, C., Xu, D., Zou, J., Zhuang, Z., Wang, Q., 2011. 'Green tides' are overwhelming the coastline of our blue planet: taking the world's largest example. Ecol. Res. 26, 477–485.
Zhang, J., Huo, Y., Wu, H., Yu, K., Kim, J.K., Yarish, C., Qin, Y., Liu, C., Xu, R., He, P., 2014. The origin of the Ulva macroalgal blooms in the Yellow Sea in 2013. Mar. Pollut. Bull. 89, 276–283.
Zhang, J., Huo, Y., Yu, K., Chen, Q., He, Q., Han, W., Chen, L., Cao, J., Shi, D., He, P., 2013. Growth characteristics and reproductive capability of green tide algae in Rudong coast, China. J. Appl. Phycol. 25, 795–803.